**Turkish Computational and Theoretical Chemistry**

*Turkish Comp Theo Chem (TC&TC)*

***Volume(Issue): 7(2) – Year: 2023 – Pages: 12-19***

***e-ISSN: 2602-3237***

***https://doi.org/10.33435/tcandtc.1161253***

***Received:*** 12.08.2022 ***Accepted:*** 01.11.2022 *Research Article*

# *A class of two-dimensional WSeTe monolayers under pressures with novel electronic and optical properties*

**Idrees Oreibi[1], Jassim M.AL-Issawe**

Directorate of Education Babylon, Ministry of Education, Iraq

**Abstract:** *The electronic and optical properties of the WSeTe monolayer have already been evaluated at different hydrostatic pressures up to 9 GPa using a first principles simulation based on dft. At all pressures, the material is semi-conductive and the band gap narrows. The examination of optical functions demonstrates that the WSeTe monolayer's absorption increases significantly as we travel towards the violet region as well as conductivity, making it useful in solar cells. All optical qualities increase as a result of the applied pressure. We contend that the extraordinary photovoltaic properties of the WSeTe monolayer have many applications in optical devices.*

***Keywords:*** DFT, Optical properties, Monolayer

## 1. Introduction

Two-dimensional (2D) materials moved to the center of material research shortly following the discovery of graphene in 2004[1, 2]. Graphene has spurred substantial research into two-dimensional (2D) materials such as MXenes [3], silicene [4], MXY Janus [5-7], germanene[8], III-group monochalcogenides [9, 10], phosphorene [11], and stanine [12] due to the outstanding mechanical and electronic properties such as high carrier mobility and high ambient stability [13, 14], which are applicable in optoelectronics [15, 16], photocatalytic water splitting [17, 18], spintronics [19], gas sensors [20], catalysts [21], transistors [22], valleytronic devices [23], quantum spin Hall insulator [24]. A novel class of materials called Janus 2D materials exhibits unusual physical, chemical, and quantum characteristics, such as significant Rashba effects and out-of-plane piezoelectric polarization, as a result of their out-of-plane asymmetry [25, 26]. The highly desired vertical piezoelectric effect is present in Janus MXY monolayers, which could significantly boost the operability and compatibility of piezoelectric devices [13]. By sulfurization in $MoSe_2$ or selenization in $MoS_2$, the polar Janus MXY monolayer (M = Mo,W; X,Y = S,Se,Te) has been effectively produced [14]. Recently, the CVD technique has been used to successfully produce Janus MXY (M=Mo,W; X=Y=Se,S,Te) monolayers in high-quality samples [27].

In this work, we utilize first-principles simulations to investigate how pressure influences the electronic and optical characteristics of Janus MXY semiconductors (WSeTe). Compared to traditional bulk semiconductors, 2D semiconductors(2DSCs) have better mechanical characteristics [28].

Global research communities in physics, engineering, chemistry, and materials have all given 2DSCS a lot of attention recently [29], 2DSCs are desirable candidates for application in a number of electrical and photonic devices due to their distinct optoelectronic features [30], including photovoltaic cells [31, 32], photodetectors [33, 34], and LED [34], These substances are atomically thick natural semiconductors [35].

Compared to other wide-band-gap Janus systems, WSeTe has a better visible-light absorption efficiency. the electron and hole mobilities of WSeTe monolayer arrive at 245 and 606 $cm^2V^{-1}s^{-1}$ to 182 and 394 $cm^2V^{-1}s^{-1}$, respectively [36]. These characteristics make the WSeTe monolayer an

[1] Corresponding Authors

e-mail: idrees114af@gmail.com

intriguing scientific study topic. The purpose of our current research is to apply varying hydrostatic pressures to the WSeTe monolayer in order to lower the band gap, which may enhance the optical absorption and performance of optoelectronic devices.

## 2. Computational Method

In this study, we calculate the optical and electronic properties of the WSeTe monolayer by first-principles calculations using castep code [37], with the generalized gradient approximations (GGA) [38]. In the current work, the exchange-correlation energy functional developed by Perdew, Burke, and Ernzerhof (PBE) has been applied. The interaction of valence electrons is defined by the ultrasoft pseudopotential [39]. 500 eV was chosen as the cutoff energy for the plane-wave basis. The 4x4x1 supercell is the model system used in this work to replicate the WSeTe monolayer, The relativistic treatment follows out via the function of Koelling-Harmon. The computations' self-consistent energy tolerance was determined to have converged at 4E-6 eV/atom, while the force's convergence threshold was established at 0.015 eV/Å. A vacuum gap of 20 Å along the perpendicular direction to the surface was utilized to exclude the interaction between two adjacent layers. To compute the geometry optimization and optical characteristics, respectively, the Brillouin zone is integrated with a 16x16x1 and 18x18x1 Monkhorst-Pack k-point mesh [40].

## 3. Results and discussion

### 3.1. Structural and electronic properties

Figure 1 shows the geometrical atomic structures of WSeTe monolayers from various angles. At equilibrium, WSeTe monolayers correspond to the space group P3m1. One Te layer, one W layer, and one Se layer are stacked in the z direction to form the monolayer WSeTe. Janus asymmetry is one of the distinctive aspects of the WSeTe monolayer, in which the structural imbalance in the WSeTe monolayer violates the typical reflection symmetry in the out-of-plane direction. Notably, the symmetry of Janus WSeTe in 2H phase is lower than that of MoSe2 and MoTe2 monolayers, despite the similarity of their structures.

To prevent any interaction between neighboring atom layers, the monolayer WSeTe is created with a vacuum area height of over 20 Å, The thickness of WSeTe is 3.495 Å. According to our calculations, as shown in table 1, the optimized lattice constants and bond length of the monolayer WSeTe drop as pressure rises. There are no experimental data on structural characteristics to be utilized as a reference, although our calculated values are comparably close to those of Sun et al [41].

We note in Figure 2, as the pressure increases, the valance band maximum and conduction band minimum begin to shift toward Ef. As a result, the band gap of the WSeTe monolayer decreases with an increase in pressure; consequently, the transition of excited electrons from the valance band to the conduction band becomes much easier and faster. When the pressure increases to 3GPa, the direct bandgap is transferred to the indirect bandgap, this corresponds to the previous theoretical report [42]. The material is a semiconductor at 0,3,9 GPa with an indirect energy gap of 1.19 eV and 0.99 eV at 0 and 9 GPa and a direct energy gap of 1.38 eV at 0 GPa, this values comparably close to previous theoretical reports [41]. The conduction band's lowest bottom and valence band's highest peak are located between H and K under pressure 0 GPa, but at pressures 3 GPa and 9 GPa, the valence band's highest peak is at H and the conduction band's lowest bottom is between K and G. The total and partial density of states (PDOS) of the WSeTe monolayer at different pressures are depicted in Figure 3. Unquestionably, a thorough examination of the Figures reveals the deportment of PDOS curves at the various pressures investigated. It indicates that the pattern is very similar, if not identical, with only a small change in peak height and form. The diagrams demonstrate that the valence band and conduction band around the fermi level (near zero) are composed of the p orbitals of selenium and tellurium atoms and the d orbitals of tungsten. The s orbital of selenium and tellurium atoms, as well as the p orbital of tungsten atoms, govern the distant section of the conduction band. The s orbital of selenium and tellurium atoms govern the furthest portion of the valence band. The findings are the best reinforcement for the band structure's results.

Table 1. The lattice constants and bonds length of the monolayer WSeTe at a different pressure.

| **pressure** | a=b Å | c Å | $d_{Te-W}$ Å | $d_{Se-W}$ Å |
|---|---|---|---|---|
| **0GPa** | **3.428** | **19.139** | **2.740** | **2.544** |
| **3GPa** | **3.352** | **7.88** | **2.729** | **2.527** |
| **9GPa** | **3.266** | **7.339** | **2.711** | **2.507** |

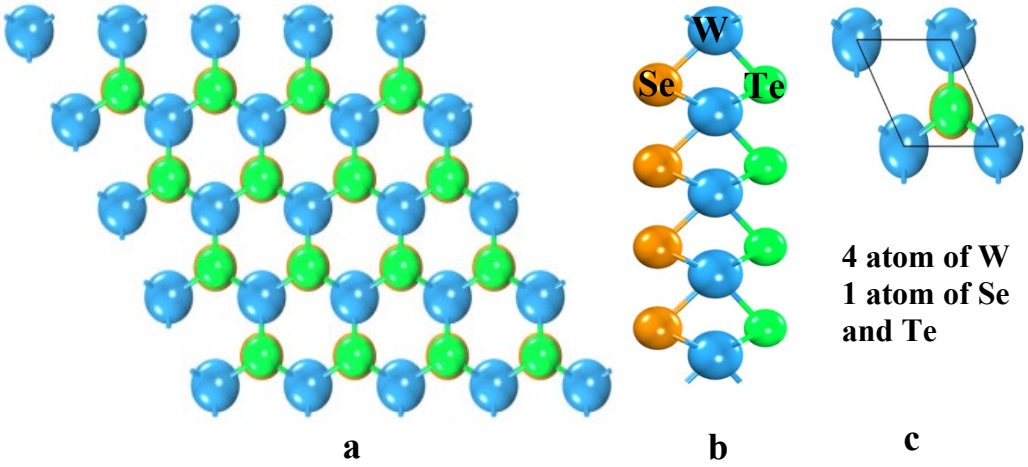


**Figure 1.** The top views (a), side views (b) and unit cell (c) of WSeTe monolayer. The green, blue, and brouwn balls are Se, W, and Te atoms, respectively.

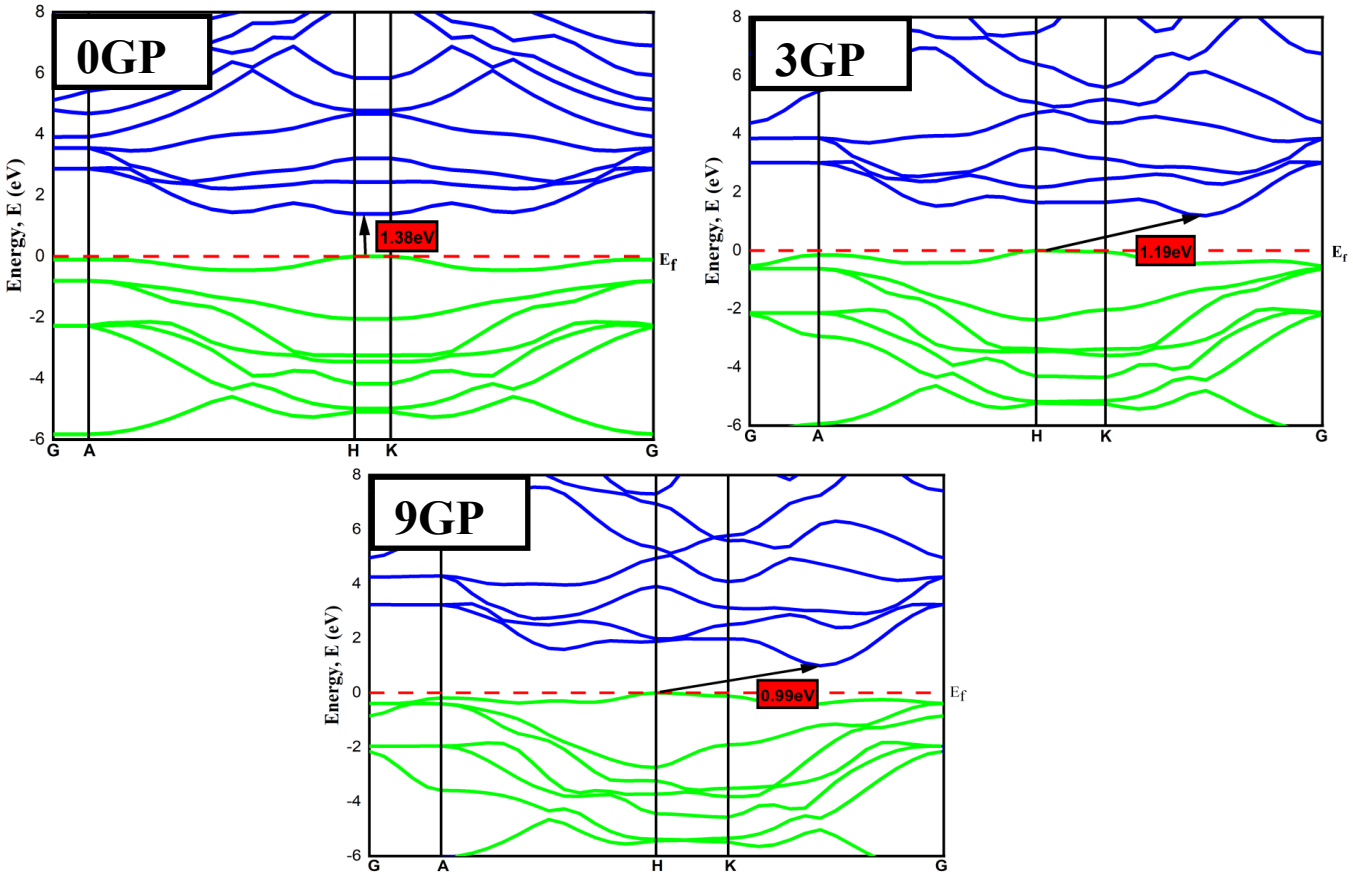


**Figure 2.** Band structure of WSeTe monolayer under different pressures.

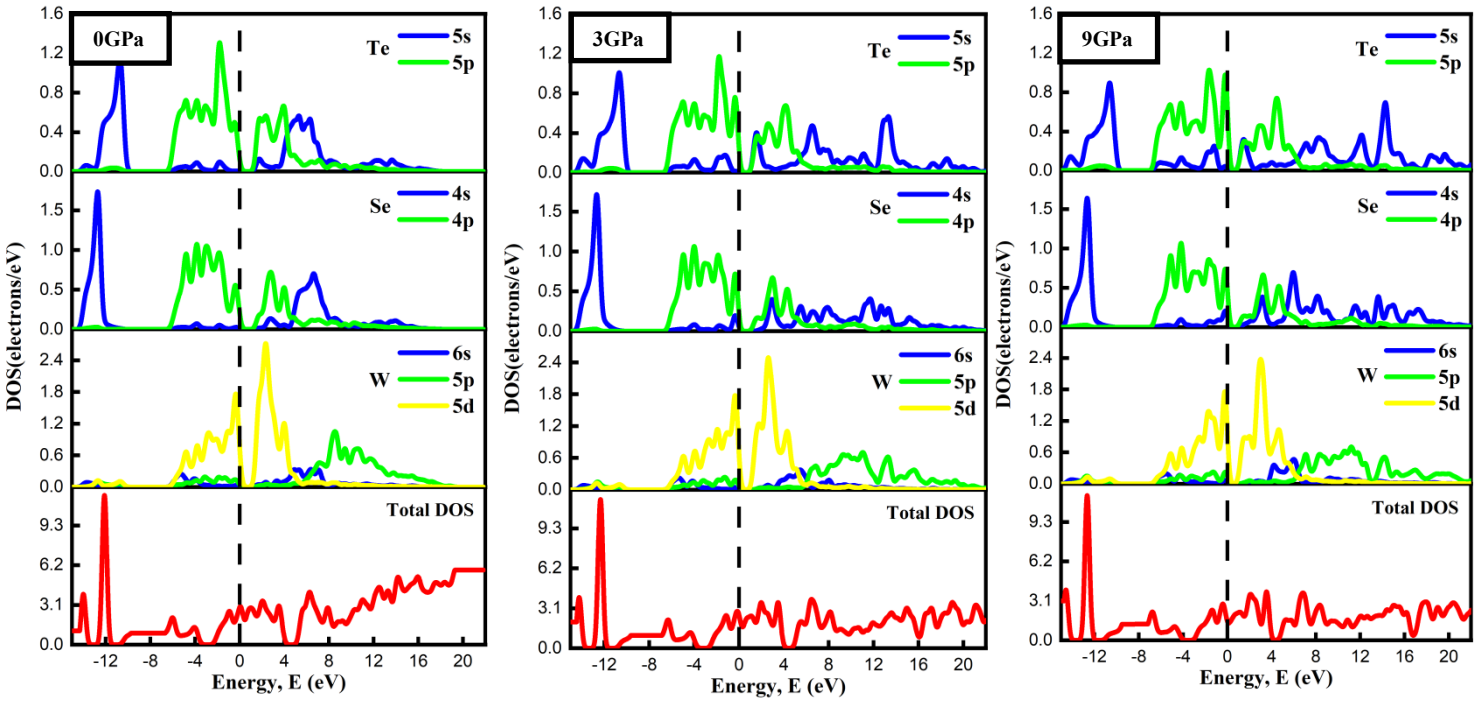


**Figure 3.** TDOS and PDOS of WSeTe monolayer under different pressures.

3.2. The optical properties

In order to determine the possible uses of a material in optical detection and electrical devices, it is essential to know its optical characteristics. In this research, the optical characteristics of WSeTe monolayers in the energy range up to 70 eV are determined.

The optical absorption depicted in Figure 4(a) begins in the infrared (IR) region at energies less than 0.01 eV for all pressures. Regarding the optical absorption in the visible area between (1.6 and 3.3) eV, which is one of the most important regions for studying the absorption of light and which may be utilized in the production of solar cells, our results highlighted a significant rise in this region. For 0GPa, 3GPa, and 9GPa, the initial optical absorption peaks are located in the ultraviolet range, precisely at energies of 5 eV. The second peaks are located in the same region for all pressures, at 11 eV. These monolayers can absorb light throughout a broad spectrum, from infrared to ultraviolet. Consequently, these 2D materials may be advantageous for photoelectric and optoelectronic devices in the aforementioned regions. Reflectivity as a function of photon energy is seen in Figure 4(b). Clearly, the static reflectivities of 0GPa, 3GPa, and 9GPa pressures (at zero energy) are 0.21, 0.36, and 0.395, respectively. There are several peaks of reflectivity, with the major peak of 0 GPa, 3 GPa, and 9 GPa pressures occurring in the ultraviolet zone at around 5 eV. The reflectivity indicated a notable degree of anisotropy in the energy range between 0 and 35 eV, which decreases gradually and becomes zero beyond 45 eV. Consequently, WSeTe monolayers may be used as a covering nanomaterial in the UV and visible spectrums. Increased pressure results in a rise in reflectance, which can reduce the efficiency of a solar cell. Consequently, greater study should be undertaken to lessen reflection [43].

The conductivity spectra under several hydrostatic pressures is illustrated in Figure 4(c), As seen in Figure 4(a), the conductivity spectrum resembles the absorption spectrum in terms of its features because when a substance absorbs energy, free carriers are released for conduction , The conductivity rises in the visible light region to reach 3.5 eV at 3 GPa and 9 GPa in the violet region, then continues to rise until it reaches its main peak at the beginning of the UV region, then decreases to a value that is practically equal to zero, before rising at 40 eV to reach approximately 4 $\mathbf{10^{15}/sec}$ at the UV zone's extremes. The real dielectric constant of the WSeTe monolayer is depicted in Figure 4(d) with the highest value appearing at 1.25 eV in the

near infrared region for all pressures and beginning to decrease in the visible light region. Its high value is approximately 8 at pressure 0 GPa and becomes 20 and 22 at 3 GPa and 9 GPa, respectively. Materials with improved dielectric constant values indicate materials with a lower incidence of charge carrier recombination and higher effectiveness in semiconductor fabrication.

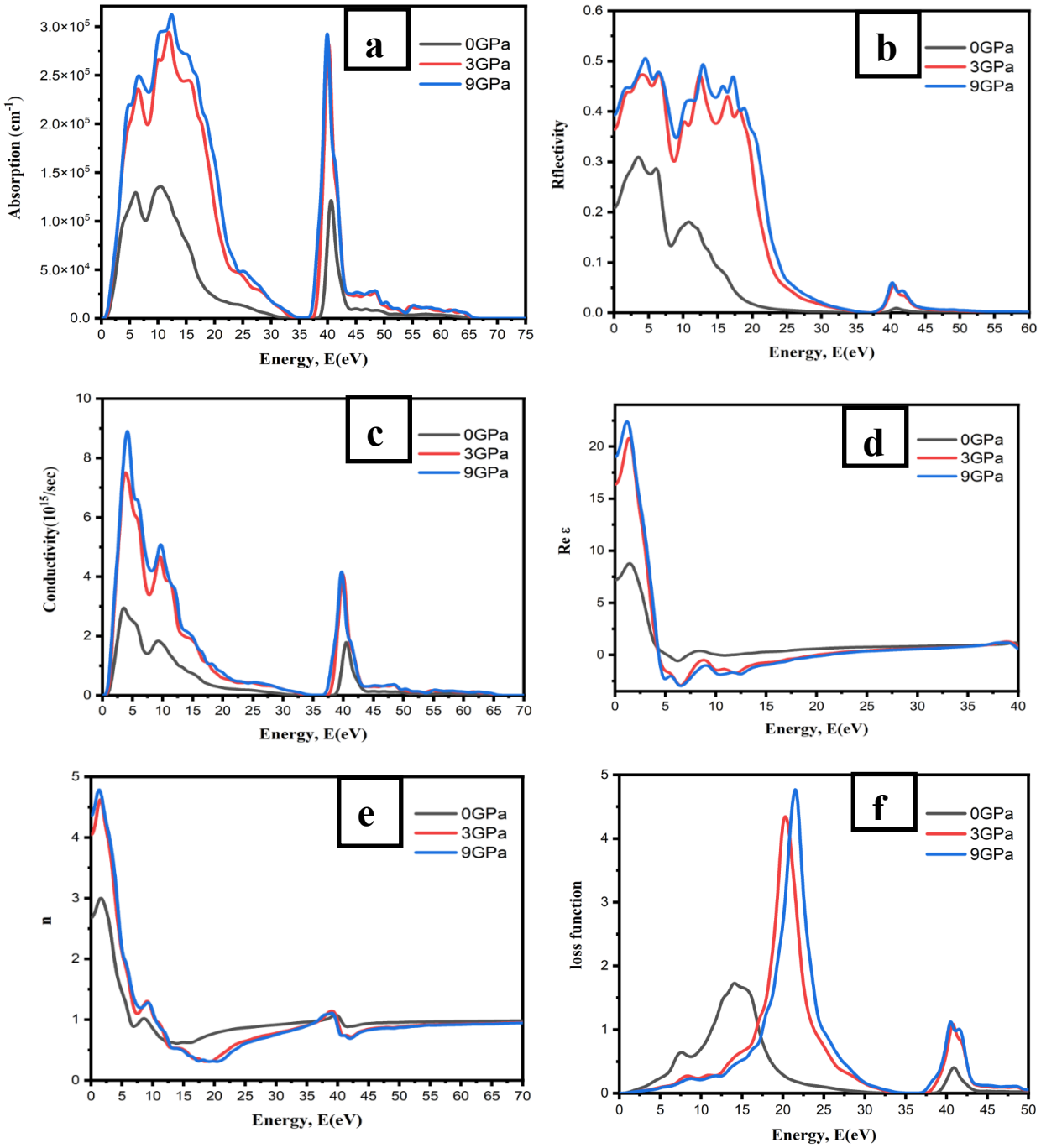


**Figure 4.** The optical properties for WSeTe monolayer under pressures: (a) the absorption, (b) the reflectivity, (c) the conductivity, (d) the real part of the dielectric function, (e) the refraction index (f) the loss function

Our findings lead us to a significant and consequential conclusion: transfers in the WSeTe monolayer are effective at all pressures. As we already know, a rise in the number of peaks indicates an increase in the number of electron transitions. More electrons are transported between

the valence and conduction bands as the number peaks increase. Higher refractive index materials provide good choices for light-trapping components in photonic crystals [44] and solar cells [45] because they have bigger scattering cross sections [46] and smaller mode volumes [47]. Evidently, in Figure 4(e), the visible light zone has the highest values of the refractive index, which are 3(0GPa), 4.6(3GPa), and 4.75. (9GPa). After then, the values of the refractive index begin to decrease until they approach a point that is nearly constant at 55 eV, at which time the refractive index is equal to 1. This suggests that when the photon energy reaches around 55 eV, this monolayer transforms from an isotropic to an anisotropic state because the difference in refractive index values (n) is close to zero.

Figure 4(f) revealed the loss function versus photon energy, this function depicts the loss of photon energy by electrons as they absorb photon energy and travel inside the material. However, the greatest peaks of the loss function are found in the ultraviolet area and have values of 1.7, 4.4, and 4.8 at 0 GPa, 3 GPa, and 9 GPa, respectively.

## 4. Conclusions

Under hydrostatic pressure, the electronic and optical properties of a WSeTe monolayer have been examined using a DFT-based CASTEP module. The pressure has a substantial effect on the WSeTe monolayer's electronic properties. The band gap decreases with increasing pressure, and the material is semiconductive at all pressures. By applying pressure, the performance of WSeTe monolayer in solar cells and other optoelectronic devices may be greatly enhanced, as indicated by the observable increase in optical absorption and conductivity in the visible spectrum. All optical characteristics, including index of refraction, dielectric constant, loss function, etc., are enhanced as a result of the applied pressure.

## References

[1] P. Nandi, A. Rawat, R. Ahammed, N. Jena, A. De Sarkar, Group-IV (A) Janus dichalcogenide monolayers and their interfaces straddle gigantic shear and in-plane piezoelectricity, Nanoscale 13 (2021) 5460-5478.

[2] H.D. Bui, H.R. Jappor, N.N. Hieu, Tunable optical and electronic properties of Janus monolayers Ga2SSe, Ga2STe, and Ga2SeTe as promising candidates for ultraviolet photodetectors applications, Superlattices and Microstructures 125 (2019) 1-7.

[3] M. Naguib, V.N. Mochalin, M.W. Barsoum, Y. Gogotsi, 25th anniversary article: MXenes: a new family of two-dimensional materials, Advanced materials 26 (2014) 992-1005.

[4] P. Vogt, P. De Padova, C. Quaresima, J. Avila, E. Frantzeskakis, M.C. Asensio, A. Resta, B. Ealet, G. Le Lay, Silicene: compelling experimental evidence for graphenelike two-dimensional silicon, Physical review letters 108 (2012) 155501.

[5] Y. Zhang, H. Ye, Z. Yu, Y. Liu, Y. Li, First-principles study of square phase MX2 and Janus MXY (M= Mo, W; X, Y= S, Se, Te) transition metal dichalcogenide monolayers under biaxial strain, Physica E: Low-dimensional Systems and Nanostructures 110 (2019) 134-139.

[6] H.G. Abbas, T.T. Debela, J.R. Hahn, H.S. Kang, Multiferroicity of Non-Janus MXY (X= Se/S, Y= Te/Se) Monolayers with Giant In-Plane Ferroelectricity, The Journal of Physical Chemistry C 125 (2021) 7458-7465.

[7] Y. Chen, H. Zhang, B. Wen, X.B. Li, X.L. Wei, W. Yin, L.M. Liu, G. Teobaldi, The Role of Permanent and Induced Electrostatic Dipole Moments for Schottky Barriers in Janus MXY/Graphene Heterostructures: a First Principles Study, Dalton Transactions (2022).

[8] C.-C. Liu, W. Feng, Y. Yao, Quantum spin Hall effect in silicene and two-dimensional germanium, Physical review letters 107 (2011) 076802.

[9] P. Li, I. Appelbaum, Symmetry, distorted band structure, and spin-orbit coupling of group-III metal-monochalcogenide monolayers, Physical Review B 92 (2015) 195129.

[10] C. Ren, S. Wang, H. Tian, Y. Luo, J. Yu, Y. Xu, M. Sun, First-principles investigation on electronic properties and band alignment of group III monochalcogenides, Scientific Reports 9 (2019) 1-6.

[11] S.P. Koenig, R.A. Doganov, H. Schmidt, A. Castro Neto, B. Özyilmaz, Electric field effect in ultrathin black phosphorus, Applied Physics Letters 104 (2014) 103106.

[12] F.f. Zhu, W.j. Chen, Y. Xu, C.l. Gao, D.d. Guan, C.h. Liu, D. Qian, S.C. Zhang, J.f. Jia, Epitaxial growth of two-dimensional stanene, Nature materials 14 (2015) 1020-1025.

[13] X. Tang, S. Li, Y. Ma, A. Du, T. Liao, Y. Gu, L. Kou, Distorted Janus transition metal

dichalcogenides: Stable two-dimensional materials with sizable band gap and ultrahigh carrier mobility, The Journal of Physical Chemistry C 122 (2018) 19153-19160.

[14] C. Xia, W. Xiong, J. Du, T. Wang, Y. Peng, J. Li, Universality of electronic characteristics and photocatalyst applications in the two-dimensional Janus transition metal dichalcogenides, Physical Review B 98 (2018) 165424.

[15] H.R. Jappor, M.A. Habeeb, Optical properties of two-dimensional GaS and GaSe monolayers, ELSEVIER RADARWEG 29(2022)1043.

[16] G. Liang, X. Yu, X. Hu, B. Qiang, C. Wang, Q.J. Wang, Mid-infrared photonics and optoelectronics in 2D materials, Materials Today 51 (2021) 294-316.

[17] Y. Li, Y.-L. Li, B. Sa, R. Ahuja, Review of two-dimensional materials for photocatalytic water splitting from a theoretical perspective, Catalysis Science & Technology 7 (2017) 545-559.

[18] G.S. Shanker, A. Biswas, S. Ogale, 2D materials and their heterostructures for photocatalytic water splitting and conversion of CO2 to value chemicals and fuels, Journal of Physics: Energy 3 (2021) 022003.

[19] X. Li, X. Wu, Two-dimensional monolayer designs for spintronics applications, Wiley Interdisciplinary Reviews: Computational Molecular Science 6 (2016) 441-455.

[20] H.R. Jappor, S.A.M. Khudair, Electronic properties of adsorption of CO, CO2, NH3, NO, NO2 and SO2 on nitrogen doped graphene for gas sensor applications, Sensor Letters 15 (2017) 432-439.

[21] 21. H.R. Jappor, A.S. Jaber, Electronic properties of CO and CO2 adsorbed silicene/graphene nanoribbons as a promising candidate for a metal-free catalyst and a gas sensor, Sensor Letters 14 (2016) 989-995.

[22] B. Radisavljevic, M.B. Whitwick, A. Kis, Integrated circuits and logic operations based on single-layer MoS2, ACS nano 5 (2011) 9934-9938.

[23] F. Bussolotti, H. Kawai, Z.E. Ooi, V. Chellappan, D. Thian, A.L.C. Pang, K.E.J. Goh, Roadmap on finding chiral valleys: screening 2D materials for valleytronics, Nano Futures 2 (2018) 032001.

[24] R. Stühler, F. Reis, T. Müller, T. Helbig, T. Schwemmer, R. Thomale, J. Schäfer, R. Claessen, Tomonaga–Luttinger liquid in the edge channels of a quantum spin Hall insulator, Nature Physics 16 (2020) 47-51.

[25] M. Yagmurcukardes, Y. Qin, S. Ozen, M. Sayyad, F.M. Peeters, S. Tongay, H. Sahin, Quantum properties and applications of 2D Janus crystals and their superlattices, Applied Physics Reviews 7 (2020) 011311.

[26] L. Zhang, Z. Yang, T. Gong, R. Pan, H. Wang, Z. Guo, H. Zhang, X. Fu, Recent advances in emerging Janus two-dimensional materials: from fundamental physics to device applications, Journal of Materials Chemistry A 8 (2020) 8813-8830.

[27] B. Hou, Y. Zhang, H. Zhang, H. Shao, C. Ma, X. Zhang, Y. Chen, K. Xu, G. Ni, H. Zhu, Room temperature bound excitons and strain-tunable carrier mobilities in janus monolayer transition-metal dichalcogenides, The journal of physical chemistry letters 11 (2020) 3116-3128.

[28] L. Gao, Flexible device applications of 2D semiconductors, Small 13 (2017) 1603994.

[29] J. Shang, C. Cong, L. Wu, W. Huang, T. Yu, Light sources and photodetectors enabled by 2D semiconductors, Small Methods 2 (2018) 1800019.

[30] J.W. Hill, C.M. Hill, Directly visualizing carrier transport and recombination at individual defects within 2D semiconductors, Chemical science 12 (2021) 5102-5112.

[31] C. Wang, Y. Jing, X. Zhou, Y.-f. Li, Sb2TeSe2 monolayers: Promising 2D semiconductors for highly efficient excitonic solar cells, ACS omega 6 (2021) 20590-20597.

[32] N. Ahmadvand, E. Mohammadi-Manesh, Engineering 2D semiconductors of PbI2@ NdI2 and NdI2@ CuI with respect of photovoltaic and solar cell applications, Surfaces and Interfaces 30 (2022) 101939.

[33] Q. Li, J. Lin, T.-Y. Liu, X.-Y. Zhu, W.-H. Yao, J. Liu, Gas-mediated liquid metal printing toward large-scale 2D semiconductors and ultraviolet photodetector, npj 2D Materials and Applications 5 (2021) 1-10.

[34] B. Wang, S.P. Zhong, Z.B. Zhang, Z.Q. Zheng, Y.P. Zhang, H. Zhang, Broadband photodetectors based on 2D group IVA metal chalcogenides semiconductors, Applied Materials Today 15 (2019) 115-138.

[35] 35. X. Song, J. Hu, H. Zeng, Two-dimensional semiconductors: recent progress and future perspectives, Journal of Materials Chemistry C 1 (2013) 2952-2969.

[36] J. Wang, H. Shu, T. Zhao, P. Liang, N. Wang, D. Cao, X. Chen, Intriguing electronic and optical properties of two-dimensional Janus transition metal dichalcogenides, Physical Chemistry Chemical Physics 20 (2018) 18571-18578.

[37] S.J. Clark, M.D. Segall, C.J. Pickard, P.J. Hasnip, M.I. Probert, K. Refson, M.C. Payne, First principles methods using CASTEP, Zeitschrift für kristallographie-crystalline materials 220 (2005) 567-570.

[38] J.P. Perdew, K. Burke, M. Ernzerhof, Generalized gradient approximation made simple, Physical review letters 77 (1996) 3865.

[39] D. Vanderbilt, Soft self-consistent pseudopotentials in a generalized eigenvalue formalism, Physical review B 41 (1990) 7892.

[40] H.J. Monkhorst, J.D. Pack, Special points for Brillouin-zone integrations, Physical review B 13 (1976) 5188.

[41] Y. Sun, Z. Shuai, D. Wang, Janus monolayer of WSeTe, a new structural phase transition material driven by electrostatic gating, Nanoscale 10 (2018) 21629-21633.

[42] H. Liu, Z. Huang, C. He, Y. Wu, L. Xue, C. Tang, X. Qi, J. Zhong, Strain engineering the structures and electronic properties of Janus monolayer transition-metal dichalcogenides, Journal of Applied Physics 125 (2019) 082516.

[43] J. Islam, A. Hossain, Semiconducting to metallic transition with outstanding optoelectronic properties of CsSnCl3 perovskite under pressure, Scientific reports 10 (2020) 1-11.

[44] J.D. Joannopoulos, P.R. Villeneuve, S. Fan, Photonic crystals: putting a new twist on light, Nature 386 (1997) 143-149.

[45] D.M. Callahan, J.N. Munday, H.A. Atwater, Solar cell light trapping beyond the ray optic limit, Nano letters 12 (2012) 214-218.

[46] M. Born, E. Wolf, Principles of optics: electromagnetic theory of propagation, interference and diffraction of light, Elsevier (2013).

[47] R. Coccioli, M. Boroditsky, K. Kim, Y. Rahmat-Samii, E. Yablonovitch, Smallest possible electromagnetic mode volume in a dielectric cavity, IEE Proceedings-Optoelectronics 145 (1998) 391-397.